DISCUSSION

The detection limit of the refractive index deviation by this technique was worse than that of other techniques [7, 11]. The visibility of the measured periodic intensity pattern was only 8%, which might reflect on the result. The low visibility is considered to be due to the MTF of the detector. Using a detector with a better MTF will raise the visibility of measured pattern and therefore improve the sensitivity to refractive index deviation. If a phase grating with a period larger than that used in this study can be used within the permitted range determined by the spatial coherency, the sensitivity to refractive index deviation will be improved as well.

The spatial resolution of the fringe scanning method is limited by the pixel size in principle. Although presented result exceeded the limit of the sampling theorem in the case of using the Fourier-transform method, the resultant value 7.5 μm was much worse than the pixel size of the image detector used. However, this result was predicted because the edge-contrast as seen in Fig. 2 caused by Fresnel diffraction is unavoidable. The amount of the blur (or the thickness of the edge contrast) is estimated to be $\sqrt{\lambda z}$ = 5.6 μm in this case. When the object can be placed downstream of the grating, this blur will be reduced. However, it should be noted that the sensitivity is proportional to distance between the object and the detector, and therefore one has to compromise the decrease in sensitivity in this case. The fractional Talbot effect occurs when the phase grating is illuminated by spherical X-rays. Therefore, another approach for reducing the blur due to Fresnel diffraction is found by combining this method with X-ray imaging microscopy. Provided that an image detector of a wide field of view compatible with a small pixel size in the future, the presented technique would be an approach for attaching a phase-contrast mode in a simple way. In addition, we consider that the combination with an X-ray imaging microscope is an important future direction of the presented method.

CONCLUSION

X-ray phase microtomography with a single phase grating was performed at BL20XU of SPring-8. An Au phase grating was placed behind an object and illuminated by spatially coherent X-rays. Periodic intensity pattern caused by the fractional Talbot effect was measured by a high resolution image detector. A differential phase map was retrieved by the fringe scanning method and phase tomograms were reconstructed. The combination with X-ray microscopy will be a next step, providing a new type differential phase microscopy, with which phase nanotomography would be attainable.

ACKNOWLEDGEMENT

The experiment using synchrotron radiation was performed under the approval of SPring-8 committee 2006A1237-NM-np. This study was financially supported by the project "Development of System and Technology for Advanced Measurement and Analysis" of Japan Science and Technology Agency (JST).

REFERENCES

1. A. Momose, *Nucl. Instrum. Methods* **352**,622-628(1995)
2. T. J. Davis, D. Gao, T. E. Gureyev, A. W. Stevenson and S. W. Wilkins: *Nature* **373**,595-598(1995)
3. A. Snigirev, I. Snigireva, V. Kohn, S. Kuznetsiv and I. Schelov, *Rev. Sci. Instrum.* **66**, 5486-5492 (1995)
4. C. David, B. Nöhammer, H. H. Solak and E. Ziegler: *Appl. Phys. Lett.* **81**, 3287-3289(2002)
5. A. Momose, S. Kawamoto, I. Koyama, Y. Hamaishi, K. Takai and Y. Suzuki: *Jpn. J. Appl. Phys.* **42**, L866-L868(2003)
6. T. Weitkamp, B. Nöhammer, A. Diaz, C. David, F. Pfeiffer, M. Stampanoni, P. Cloetens and E. Ziegler: *Appl. Phys. Lett.* **86**, 054101(2005).
7. A. Momose, S. Kawamoto, I. Koyama and Y. Suzuki, *SPIE Proc.* **5535** , 352-360 (2004)
8. E. Pfeiffer, T. Weitkamp, O. Buck and C. David, *Nature Phys.* **2**, 258-261(2006)
9. J. P. Guigay: *Opt. Acta* **18**, 677-682(1971)
10. K. A. Stetson and W. R. Brohinsky: *Appl. Opt.* **24**, 3631-3637(1985)
11. A. Momose, A. Fujii, H. Kadowaki and H. Jinnai: *Macromolecules* **38**, 7197-7200(2005)

Phase Tomography Using X-ray Talbot Interferometer

A. Momose,[1] W. Yashiro,[1] Y. Takeda,[2] M. Moritake,[1]
K. Uesugi,[3] Y. Suzuki,[3] and T. Hattori[4]

[1]*Graduate School of Frontier Sciences, The University of Tokyo, 5-1-5 Kashiwanoha, Kashiwa, Chiba 277-8561, Japan*
[2]*Graduate School of Pure and Applied Sciences, University of Tsukuba, 1-1-1 Tennodai, Tsukuba, Ibaraki 305-8573, Japan*
[3]*SPring-8/JASRI, 1-1-1 Kouto, Mikazuki, Hyogo 679-5198, Japan*
[4]*Laboratory of Advanced Science and Technology for Industry, University of Hyogo, 3-1-2 Kouto, Kamigori, Hyogo 678-1205, Japan*

Abstract. A biological tomography result obtained with an X-ray Talbot interferometer is reported. An X-ray Talbot interferometer was constructed using an amplitude grating fabricated by X-ray lithography at the LIGA beamline of NewSUBARU and gold electroplating. The pitch and pattern thickness of the grating were 8 μm and 30 μm, respectively. The effective area was 20 × 20 mm^2, which was entirely illuminated with a wide beam available at the medium-length beamline 20B2 of SPring-8, allowing the acquisition of a three-dimensional tomogram of almost the whole body of a fish. The resulting image obtained with 17.7 keV X-rays revealed organs with bones in the same view.

Keywords: Tomography, Phase, Talbot effect, Talbot interferometer, Grating, High aspect ratio.
PACS: 07.05.Pj, 07.85.Tt, 41.50.+h, 42.25.Hz, 42.30.-d, 42.30.Wb,

INTRODUCTION

Recently, X-ray transmission gratings have been implemented in novel phase-sensitive X-ray imaging [1-6]. Differential phase contrast can be generated by aligning two transmission gratings on an optical axis with a specific separation determined by the pitch of the gratings and X-ray wavelength. The first grating generates self-images that exhibit periodical intensity patterns corresponding to the transmission function of the grating. The self-images are induced by Fresnel diffraction by the grating, which is known as the fractional Talbot effect. When a phase object is placed in the path of X-rays, X-ray refraction at the phase object is reflected on the deformation of the self-images. The second grating, which is of the amplitude type with a pitch almost the same as the average period of a self-image and is placed at the position of the self-image, generates a moiré pattern by superposition with the deformed self-image. This system is known as a Talbot interferometer [7,8].

Because of its use of grating optics, Talbot interferometry has many advantages over other phase-sensitive X-ray imaging methods. One advantage is that the setting up of a Talbot interferometer is easy because gratings can be aligned with an accuracy corresponding to their pitch, which is set to be comparable to the X-ray spatial coherence length typically on the micrometer order. Another advantage is that a cone beam with a broad energy bandwidth (approx. $E/\Delta E > 10$) can be used. In addition, it should be emphasized that the quantitative measurement of a differential phase image is feasible, enabling phase tomography.

In this paper, we describe a biological imaging result obtained by phase tomography using the X-ray Talbot interferometer at SPring-8. An amplitude grating 8 μm in pitch and 30 μm in thickness was fabricated by means of X-ray lithography and gold electroplating. Its effective area was 20 × 20 mm^2, which was covered with the wide beam of the beamline 20B2.

CP879, *Synchrotron Radiation Instrumentation: Ninth International Conference*,
edited by Jae-Young Choi and Seungyu Rah

X-RAY TALBOT INTERFEROMETER

Figure 1 shows a calculated X-ray intensity downstream from a $\pi/2$ phase grating under plane-wave illumination of X-rays of wavelength λ. The spatial coherence length of the X-rays at the grating was assumed to be almost $3d$, where d is the pitch of the grating. At the positions given by $m\lambda/4d^2$, where m is an integer other than those which are multiples of four, rectangular periodic patterns (self-images) of period d are formed in a process known as the fractional Talbot effect. The visibility of the self-images decreases along the optical axis owing to the finite spatial coherence length.

When a phase object is placed in front of the grating, the self-images are deformed due to the refraction at the phase object. The amount of deformation is proportional to the distance the self-image from the grating. In a Talbot interferometer, an amplitude grating of period d is placed at the position of one of the self-images. Then, the deformation of the self-image is visualized as a moiré pattern induced by the superposition of the self-image and amplitude grating (see Fig. 2). In the experiment presented in this paper, we selected the position corresponding to $m = 2$, where the visibility of the self-image is at its maximum.

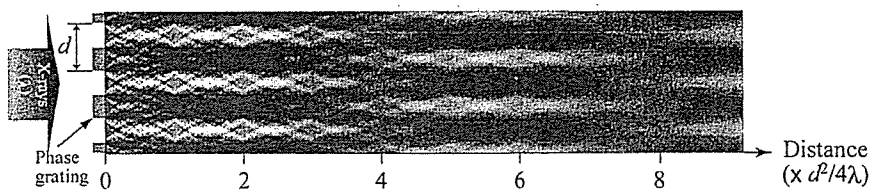

FIGURE 1. Calculation of intensity downstream of $\pi/2$ phase grating induced by fractional X-ray Talbot effect under assumption of illumination of nearly plane-wave X-rays with spatial coherence length of $3d$.

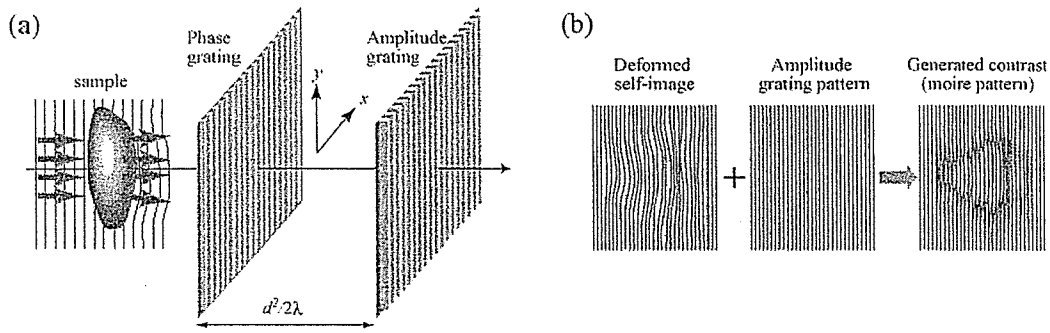

FIGURE 2. Configuration of Talbot interferometer (a) and schematic diagram (b) explaining moiré pattern generation.

The second grating used in the Talbot interferometer must, in principle, be of the amplitude type. The pattern of the grating should therefore be thick enough to absorb X-rays fully. Gold is a suitable material for this grating, considering its absorption coefficient and fabrication process. Nevertheless, a thickness much larger than 10 μm is required. The pitch of the grating should be comparable to or smaller than the spatial coherence length of X-rays to induce the fractional Talbot effect. The spatial coherence length of hard X-rays from a storage ring is typically 10 μm. Therefore, a pattern of high aspect ratio should be fabricated. We used such an amplitude grating fabricated by X-ray lithography and gold electroplating.

A 30-μm-thick X-ray resist film (MAX001, Nagase ChemteX) was spin-coated on a 200-μm-thick Si wafer with a 0.25-μm-thick Ti layer. The beamline 11 of NewSUBARU, Japan, which is dedicated to Lithographie Galvanoformung Abformung (LIGA) fabrication, was used for X-ray exposure through an X-ray mask of an 8-μm-pitch 1:1 line-and-space pattern. After developing, gold lines were formed by electroplating between resist lines, which were left after the electroplating to support the gold lines. The height of the gold lines was nearly 30 μm, and the effective area of the grating was 20 × 20 mm^2. The first grating was of the $\pi/2$ phase type for 20 keV X-rays. The basic performance of the set of gratings was reported elsewhere [6]: the visibility of moiré fringes was about 80% at 20 keV; it was greater than 30% at 31 keV.

A wide beam of the beamline 20B2 of SPring-8, Japan through a Si 111 double-crystal monochromator was used 206 m from a bending section, and the entire effective area of the gratings was illuminated by the beam. The spatial coherence length of the X-rays at the interferometer was calculated to be about 20 μm.

A CCD camera (C4742-95HR, Hamamatsu Photonics) lens-coupled with a phosphor screen was used to record moiré fringes. Its effective pixel size was 11.8 μm × 11.8 μm. A cell filled with formalin was placed close to the upstream side of the phase grating, and a sample was immersed in formalin. For tomography, the sample was rotated about the vertical axis. The lines of the gratings were also aligned vertically (parallel to the y-axis in Fig. 2(a)), such that the refraction in the horizontal plane was sensed.

Quantitative measurement of the angular beam deflection induced by the refraction at the sample, that is, a differential phase image, was carried out by observing the change in moiré patterns with the displacement of the amplitude grating in the x-direction (see Fig. 2(a)). The step of the displacement was $d/5$ and five moiré patterns were used to calculate a differential phase image using the fringe scanning method [9]. This measurement was repeated for every angular position of the sample rotation in tomography.

PHASE TOMOGRAM

Figure 3(a) shows the result of the measurement of a differential phase image of a fish (*Hasemania nana*) 3 cm in length obtained with 17.7 keV X-rays. This image was calculated from five moiré patterns, one of which is shown in Fig. 3(b). The contribution of moiré fringes appearing in the background in Fig. 3(b), which was mainly due to the pitch mismatch between the amplitude grating and the self-image, was removed using the data obtained in the absence of the sample.

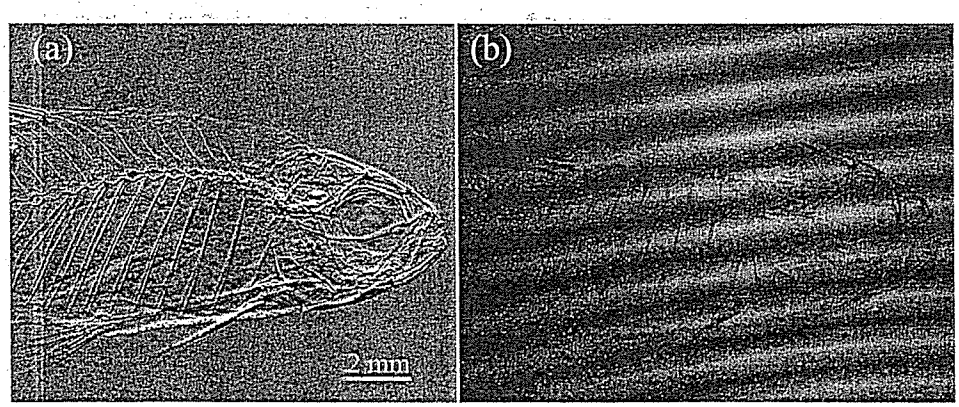

FIGURE 3. Differential phase image (a) of fish (*Hasemania nana*) calculated from a series of moiré patterns, one of which is shown in (b), recorded by fringe scanning. The X-ray energy was 17.7 keV. The vertical direction in these pictures corresponds to the x-direction in Fig. 2(a).

The angular step of the sample for phase tomography was 0.36°, and 500 differential phase images were recorded. The exposure time for obtaining a moiré image was 8.2 s. Before the tomographic reconstruction using the convolution-backprojection algorithm, each differential phase image was converted to a phase image through integration. Figure 4 shows sectional images generated using reconstructed three-dimensional data. Although artifacts remain because strong refractions at the bones and body surface could not be processed correctly within the assumption in the theory of X-ray Talbot interferometry that we used [2,9], organ structures are clearly revealed with bones in the same view, showing a wide dynamic range.

CONCLUSION

Thus, X-ray Talbot interferometry exhibited an excellent sensitivity to soft structures. As for the spatial resolution, the pitch of the gratings gives a limit. Because a cone-beam is available with an X-ray Talbot interferometer, a next possible progress is in combining such an interferometer with a normal X-ray imaging microscope as an attachment for use in a phase-contrast mode. Another possibility of progress, with which X-ray Talbot interferometry will prove its full merit, is the development of an X-ray imaging apparatus for practical

applications such as medical diagnosis not only with synchrotron radiation sources but also with compact X-ray sources. For this purpose, we need to move to a higher-energy region, and the thickness and effective area of the amplitude grating should therefore be increased.

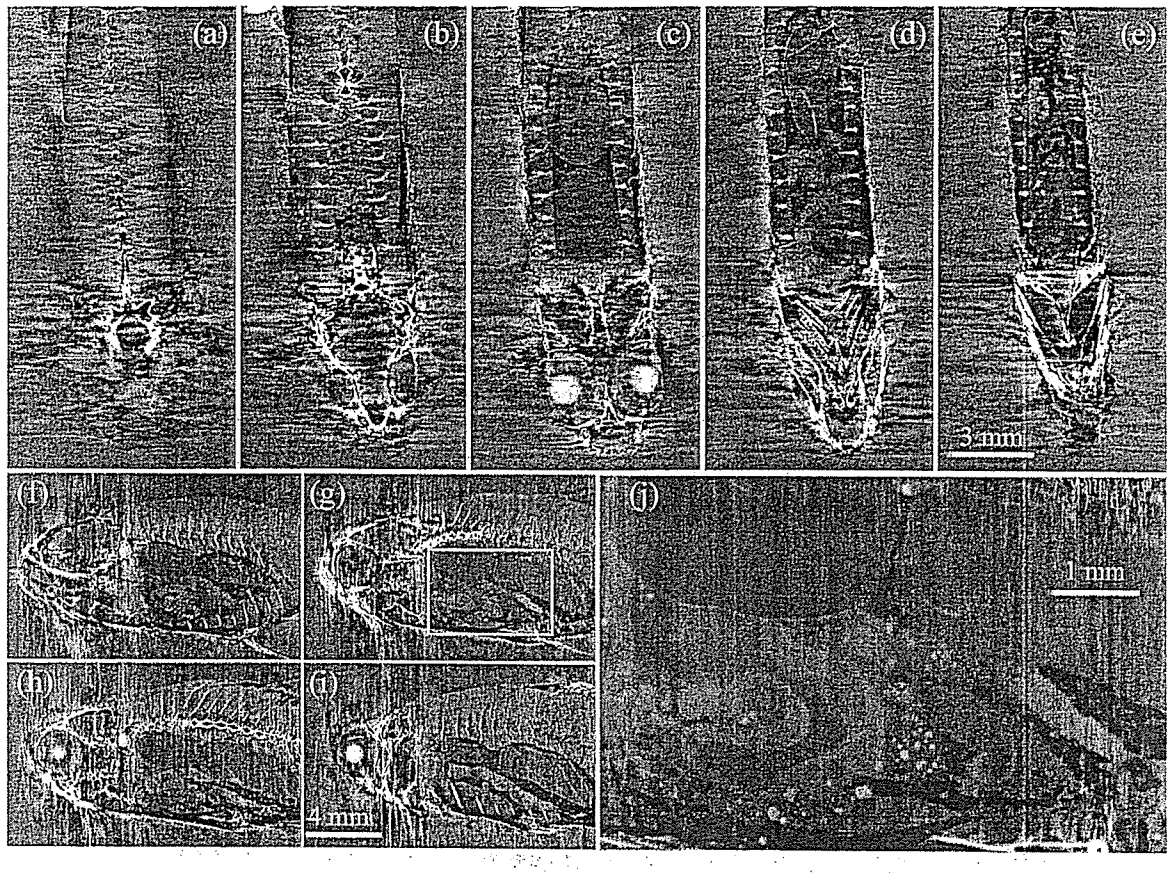

FIGURE 4. Phase tomograms of fish (*Hasemania nana*): coronal views (a)-(e) from back to stomach at 1.18 mm intervals and sagittal views (f)-(i) at 0.59 mm intervals. (j) is a magnified image of the area indicated by a rectangle in (g). Images map the refractive index difference from that of formalin ranging from -1×10^{-7} to 1×10^{-7}.

ACKNOWLEDGMENTS

The experiment using synchrotron radiation was performed under the approval of the SPring-8 committee 2006A1237-NM-np. This study was financially supported by the project "Development of System and Technology for Advanced Measurement and Analysis" of Japan Science and Technology Agency (JST).

REFERENCES

1. C. David, B. Nöhammer, H. H. Solak, and E. Ziegler, *Appl. Phys. Lett.* **81**, 3287-3289 (2002).
2. A. Momose, S. Kawamoto, I. Koyama, Y. Hamaishi, K. Takai, and Y. Suzuki, *Jpn. J. Appl. Phys.* **42**, L866-L868 (2003).
3. T. Weitkamp, B. Nöhammer, A. Diaz, and C. David, *Appl. Phys. Lett.* **86**, 054101 (2005).
4. T. Weitkamp, A. Daiz, C. David, F. Pfeiffer, M. Stampanoni, P. Cloetens, and E. Ziegler, *Opt. Express* **13**, 6296-6304 (2005).
5. F. Pfeiffer, T. Weitkamp, O. Buck, and C. David, *Nature Phys.* **2**, 258-261 (2006).
6. A. Momose, W. Yashiro, Y. Takeda, Y. Suzuki, and T. Hattori, *Jpn. J. Appl. Phys.* **45**, 5254-5262 (2006).
7. S. Yokozeki and T. Suzuki, *Appl. Opt.* **10**, 1575-1580 (1971).
8. A. W. Lohmann and D. E. Silva, *Opt. Commun.* **2**, 413-415 (1971).
9. A. Momose, S. Kawamoto, I. Koyama, and Y. Suzuki, *SPIE Proc.* **5535**, 352-360 (2004).